PNAS
www.pnas.org

Supplementary Information for

Tissue plasminogen activator promotes white matter integrity and functional recovery in a murine model of traumatic brain injury

Yuguo Xia, Hongjian Pu, Rehana K. Leak, Yejie Shi, Hongfeng Mu, Xiaoming Hu, Zhengyu Lu, Lesley M. Foley, T. Kevin Hitchens, C. Edward Dixon, Michael V. L. Bennett, and Jun Chen

Corresponding authors: Michael V. L. Bennett and Jun Chen
Email: michael.bennett@einstein.yu.edu (M.V.L.B.), chenj2@upmc.edu (J.C.).

This PDF file includes:

www.pnas.org/cgi/doi/10.1073/pnas.1810693115

Supplementary Methods

Animals were housed in a temperature and humidity-controlled facility with a 12-h light/dark cycle. Food and water were available *ad libitum*. All experimental procedures were approved by the University of Pittsburgh Institutional Animal Care and Use Committee and performed in accordance with the *NIH Guide for the Care and Use of Laboratory Animals* (1). All efforts were made to minimize animal suffering and the number of animals used.

Traumatic brain injury model.

TBI was elicited by unilateral controlled cortical impact (CCI), as previously described, with some modifications (2). Briefly, animals were randomly assigned to the CCI or sham injury group. Mice were anesthetized with 5% (vol/vol) isoflurane in a 67% (vol/vol) N_2O/30% (vol/vol) O_2 mixture through an induction chamber and this was maintained during surgery with 1.5% (vol/vol) isoflurane delivered through a nose cone. Under anesthesia, mouse heads were stabilized in a stereotaxic frame and a skin incision was made under aseptic conditions to expose the skull and Bregma. A right parietal craniotomy (centered 0.5 mm anterior and 2.0 mm lateral to Bregma; diameter of 3.5 mm) was prepared with a drill to expose the dura and cerebral cortex. CCI was performed with a pneumatically-driven CCI device (Precision Systems and Instrumentation, Fairfax Station, VA, USA) utilizing a 3 mm (diameter) flat-tipped impactor to compress the exposed brain tissue to a depth of 1.5 mm for dwell time of 150 ms at a peak velocity of 3.5 m/s. Rectal temperature was recorded and maintained at 37±0.3°C during surgery. As determined in 10 randomly selected mice, rectal temperature remained within the normal range up to 6 h after CCI. After surgery, the skin incision was sealed, and mice were placed in a clean cage. Animals in sham groups were subjected to anesthesia, skin incision, and recovery, but were not subjected to craniotomy preparation or CCI.

A total of 355 mice were used in this study. One WT mouse and one tPA KO mouse died at 5 days after TBI. One sham mouse drowned in the water maze test. These three animals were excluded from any outcome analyses. The distribution of deaths across groups and the low frequency of mortality (3/355 mice) do not support any systemic lethal effect of genotype that might have biased our interpretations.

Intranasal recombinant tPA administration.

Animals were randomly assigned to receive PBS or recombinant tPA treatment 2 h after TBI (day zero) and subsequently every other day for 14 days post-surgery. All mice were anesthetized as described above and placed in a supine position with dorsal side down. tPA (Actilyse, Boehringer Ingelheim company, Germany) was freshly dissolved in PBS (1 μg/μL) and delivered at a dose of 0.5 mg/kg. tPA was applied into each nostril 5 times (~3 μL into each nostril for each trial) with an intertreatment interval of 5 min. Animals in the vehicle control group received an equal volume of sterile PBS using the same regimen. For a 30 g mouse, we would have injected 15 μL of tPA or an equivalent volume of PBS over the course of ~25 min.

Behavior tests.

Rotarod test. The rotarod test was used to evaluate sensorimotor balance and coordination, as previously described (3). Briefly, mice were forced to run on a rotating drum (diameter: 3.2 cm; IITC Life Science Inc., Woodland Hills, CA, USA) beginning at 4 rpm and accelerating to 40 rpm in 300 seconds. The latency to fall off the drum was recorded by an investigator blinded with

respect to animal treatment. All mice were tested 4 times on each testing day, with a rest period of at least 5 min between tests. The latencies from trials 2 to 4 were then averaged. Mice were pre-trained for 3 days before surgery, and the average latency to fall on the last day before surgery was used as the baseline value. After surgery, rotarod tests were performed on days 3, 5, 7, 10, 14, 21, 28 and 35.

Cylinder test. The cylinder test was employed to assess forelimb asymmetry before and after TBI (4). Mice were placed for 10 min in a transparent cylinder 9 cm in diameter and 15 cm in height and videotaped from above. In exploring the cylinder, mice exhibit spontaneous rears contacting the cylinder wall with the right limb (R), the left limb (L), or both limbs (B). Mice that exhibited fewer than 10 rears or preference for either limb before TBI were excluded from further analyses. Behavior was recorded by an investigator blinded to groups. As the lesion was in the right hemisphere, the preference for the unimpaired right forelimb (asymmetric rate) was calculated by the following formula (R-L)/(R+L+B) × 100%. Before CCI, all mice were placed in the cylinder to establish a baseline asymmetry score.

Morris water maze test. The Morris water maze test was employed for 3 days before CCI and then from day 29 to day 34 after CCI, as described previously (4). Briefly, a square Plexiglas platform (11 × 11 cm) was submerged 1.5 cm under the surface of the water in the center of one quadrant of a circular pool (diameter: 109 cm; depth: 33±0.5 cm). Prominent spatial cues were displayed around the room. Nontoxic, white tempera paint was added to the water and the pool was maintained at a temperature of 20±1°C. The test was composed of a spatial acquisition phase to assess learning capacity and a spatial retention phase to assess memory function. For the former, the mouse was placed in the pool in one of the three quadrants without the platform and allowed to swim for 60 seconds to find the hidden platform. This test was administered 3 days before CCI to habituate the mice to swimming and from days 29 to 33 after CCI. The time spent finding the hidden platform was recorded as the latency to escape from the forced swimming task, and the mean latency of three trials was quantified as a measure of spatial learning. At the end of each trial, the mouse was placed on the platform for 30 seconds. Spatial memory was evaluated on day 34 after CCI by removing the hidden platform. Each mouse was placed in the pool once for a single 60-second-long probe trial. The time spent swimming in the goal quadrant—where the platform was previously located—was recorded as spatial memory and expressed as a percentage of the total testing time. The swim speed of each mouse was also recorded every day to assess gross motor skills.

Tract-tracer injections and quantification of axonal sprouting.

At day 21 after CCI, mice were anesthetized and stabilized in a stereotaxic frame with the skull exposed. The tract tracer biotinylated dextran amine (BDA; Thermo Fisher Scientific, D1956) was dissolved in PBS at a concentration of 10% (wt/vol) and 2 µLs were injected at two sites in the contralesional cortex (coordinates: 1. Anteroposterior (AP) 0.6 mm, mediolateral (ML) 1.2 mm, dorsoventral (DV) 1.5 mm; 2. AP 0.0 mm, ML 1.8 mm, DV 1.70 mm). Two weeks later, the brain and spinal cord were harvested after cardiac perfusion with 0.9% (wt/vol) NaCl followed by 4% (wt/vol) paraformaldehyde (PFA; Sigma-Aldrich, St. Louis, MO, USA) in PBS. Coronal brain sections and transverse cervical spinal cord sections were cut at 25 µm thickness on a cryostat (CM1900, Leica) after cryoprotection in 30% (wt/vol) sucrose in PBS. Brain sections at the level of the facial nucleus (corticobulbar projection) and sections from cervical spinal cord segment 7 (corticospinal projection) were incubated in streptavidin-FITC to label BDA^+ axons. The number of midline-crossing BDA^+ fibers (from intact to denervated side) was manually

counted by a blinded investigator. Three sections (approximately 50-75 μm apart) at the level of the medullary pyramids from each mouse were assessed in this manner.

Immunofluorescence staining and image analyses.

Animals were euthanized by deep anesthesia and transcardially perfused as above. Brains were harvested and sectioned as above. After a series of washes, nonspecific antibody binding was blocked with 5% (vol/vol) donkey or rabbit serum for 1 h followed by incubation in primary antibodies for 1 h at room temperature and overnight at 4°C. After more PBS washes, brain sections were incubated with donkey secondary antibodies conjugated to AlexaFluor 488 or Cy3 (1:1000, Jackson ImmunoResearch Laboratories, West Grove, PA, USA). Free-floating sections were then mounted and coverslipped with Fluoromount-G containing 4', 6-diamidino-2-phenylindole (DAPI; Southern Biotech, Birmingham, AL, USA). Alternate sections from each experimental group were incubated in all solutions except the primary antibodies to assess nonspecific antibody binding. The following primary antibodies were used: rabbit anti-myelin basic protein (MBP; 1:200; Abcam, Cambridge, MA, USA), mouse anti-nonphosphorylated neurofilaments (SMI-32; 1:1000; Calbiochem, San Diego, CA, USA), rabbit anti-beta amyloid precursor protein (β-APP; 1:250; Fisher Scientific 51-2700), rabbit anti-neurofilament 200 (NF200; 1:500; Abcam ab8135), and mouse anti-microtubule associated protein 2 (MAP2; 1:200; Millipore MAB3418).

Fluorescence images were captured with an inverted Nikon Diaphot-300 fluorescence microscope equipped with a SPOT RT slider camera and Meta Series Software 5.0 (Molecular Devices) or with an Olympus Fluoview FV1000 confocal microscope and FV10-ASW 2.0 software (Olympus America). The ratio of SMI-32 to MBP fluorescence intensity was quantified, as described previously (5). In brief, two regions of interest (ROIs) in perilesional cortex and striatum and one ROI in the corpus callosum (CC) and external capsule (EC) were randomly selected and captured using the same imaging parameters. Images were analyzed by an investigator blinded to experimental groups with ImageJ software (NIH, Bethesda, MD, USA). Numbers of APP^+ spots were measured by WS Recognizer software, as described (6). Briefly, images were smoothed and fluorescent spots with diameters of 5-10 μm were automatically recognized and selected. Next, the number of APP^+ spots were automatically counted by the software and divided by the area of the field of view to yield APP density.

Measurements of brain tissue loss.

Six equally-spaced MAP2-stained coronal brain sections spanning the injury site were selected from Bregma -1.34 to +1.10 mm. Brain tissue loss was analyzed by ImageJ software and calculated with the following formula: $V_C – V_L$, where V_C is the volume of the contralateral hemisphere (left hemisphere) and V_L is the volume of all residual tissue in the ipsilateral hemisphere subjected to TBI (right hemisphere).

Diffusion tensor imaging scanning and analyses.

Diffusion tensor imaging (DTI) was used to evaluate white matter integrity after TBI (7, 8). Mice were deeply anesthetized and transcardially perfused with 0.9% (wt/vol) NaCl followed by 4% (wt/vol) PFA in PBS. *Ex vivo* brains were harvested 35 days after TBI with the skull intact, to avoid anatomical deformation, and immersed in 4% (wt/vol) PFA overnight at 4°C followed by storage in PBS. MRI was performed using a Bruker AV3HD 11.7 Tesla/89 mm vertical-bore

microimaging system equipped with a Micro2.5 gradient set capable of 1500 mT/m, a 20 mm quadrature RF resonator and ParaVision 6.0.1 (Bruker Biospin, Billerica, MA, USA). Following positioning and pilot scans, a DTI dataset was covering the entire brain was collected using a multislice spin-echo sequence with 5 A_0 images and 30 non-colinear diffusion images with the following parameters: TE/TR 22/2800 ms, 2 Averages, 160 × 160 matrix, 16 × 15 mm field of view, 25 slices, 0.5mm slice thickness, b-value = 3000 s/mm^2, and Δ/δ = 11.0/5.0 ms. DTI data was analyzed with DSI Studio software (http://dsi-studio.labsolver.org/). A single ROI was manually drawn in a blinded manner encompassing the CC and EC on the ipsilesional or contralesional hemispheres to determine fractional anisotropy (FA), axial diffusivity (AD; λII, generally sensitive to axonal integrity), and radial diffusivity (RD; $\lambda\perp$; generally sensitive to myelin integrity) (9). Directionally-encoded color (DEC), FA, and RD maps were generated by DSI Studio software.

Neurite outgrowth assay.

To optimize the effects of chondroitin sulfate proteoglycan (CSPG; Millipore CC117) on neurite outgrowth, various concentrations (2.5, 5, and 10 μg/mL) of CSPG were coated on poly-D-lysine glass coverslips in 24-well cell culture plates for 2 h. After several washes with ddH_2O, embryonic neurons were plated on top of the coverslips. The embryonic neurons were harvested from E16-18 mice, trypsinized on day *in vitro* 3 (DIV3), and plated onto the CSPG-treated coverslips at a density of 2.5×10^5 cells per coverslip. Cells were fixed after 24 h with 4% (wt/vol) PFA and double-labeled with mouse anti-Tau-1 (1:250; Millipore MAB 3420) with the Alexa 488-conjugated donkey-anti-mouse secondary antibody (1:1000; Jackson ImmunoResearch Laboratories) and the nuclear DAPI stain.

For the second series of experiments, embryonic neurons were plated as above, on coverslips previously coated with 10 μg/mL CSPG, and then incubated for 1 h on DIV2 with the epidermal growth factor receptor (EGFR) inhibitor AG1478 at 200 nM (Cell Signaling 9842S) or the corresponding vehicle. After 1 h, 10 ng/mL tPA (Abcam ab92633) or the vehicle control was applied and neuron outgrowth was visualized 48 h later as above.

Images of single neurons were captured with 40× objectives using an Olympus BX51 microscope. At least 100 neurons were analyzed under each condition for each experiment, and the average of three independent experiments were calculated. Neurite outgrowth was quantified by the semi-automated ImageJ plug-in NeuronJ, as described previously (10). Neurite traces were constructed by Imaris software (Bitplane, Belfast, United Kingdom) in a semi-automated manner. Briefly, when the manual trace is centered at the cell soma, the software recognizes positively-labeled fluorescent signals above a specified fluorescent threshold (tau staining) along the axonal pathway, and artificial tracing is then generated automatically along the neurites.

Compound action potential measurements.

Compound action potentials (CAPs) in the CC and EC area were measured as described previously (11). Briefly, mice were euthanized and decapitated followed by rapid brain harvest. Coronal brain slices (350 μm) were cut -1.06 mm posterior from Bregma on a Vibratome (Leica) and placed in pre-gassed (95% (vol/vol) O_2/5% (vol/vol) CO_2) artificial cerebrospinal fluid (aCSF; NaCl 130 mmol/L, KCl 3.5 mmol/L, Na_2HPO_4 1.25 mmol/L, $MgSO_4$ 1.5 mmol/L, $CaCl_2$ 2 mmol/L, $NaHCO_3$ 24 mmol/L, glucose 10 mmol/L; pH 7.4) for 1 h at 22°C. Brain sections were then transferred into a recording chamber where they were submerged and perfused at a constant

rate (3-4 mL/min) with aCSF at 22°C. A concentric bipolar electrode was placed into the CC approximately 0.9 mm lateral to the midline. A glass extracellular recording pipette (5 to 8 MΩ tip resistance when filled with aCSF) was placed into the EC, 0.75 mm and 1 mm from the stimulating electrode. The recordings made at 0.75 mm from the stimulating electrode were analyzed and reported. Both electrodes were placed 50-100 μm below the surface of the brain slice, with adjustments by an observer blinded to treatment groups to optimize signal. The input stimuli ranged from 0 to 2 mA (100 μs duration, delivered at 0.05 Hz). The evoked CAPs were recorded by an Axoclamp 700B (Molecular Devices) and analyzed with pCLAMP 10 software (Molecular Devices). The average waveforms of four successive sweeps in two slices per mouse were quantified. The recording shows two negative peaks conventionally referred to as N1 and N2 and three positive peaks. The amplitude of the CAPs was defined as the range from the second positive peak to the third positive peak.

Quantification of intracranial hemorrhage (ICH).

ICH volume was measured with Drabkin's reagent (Sigma, D5941), as previously described (12), 24 h after CCI. CCI was performed in tPA KO and WT mice, with or without intranasal tPA treatment (2 h after TBI and 2 h before termination). Mice were transcardially perfused 24 h after TBI with 60 mL cold 0.9% (wt/vol) NaCl, and the brain was removed and cut into coronal, 1-mm thick sections. After photographs of the sliced brains were captured, brain sections were separated into contralateral and ipsilateral hemispheres by slicing sagittally through the midline. Six ipsilateral brain sections were collected in glass tubes and 500 μL water added for homogenization, followed by sonication on ice for 1 min to lyse erythrocytes and other cells. Samples were centrifuged at 15,000 *g* for 30 min in 4°C. Supernatants were transferred to a new tube containing Drabkin's reagent, mixed well by pipetting, and incubated at room temperature for 20 min. Optical density values were measured by spectrophotometry at 540 nm and then calculated for hemorrhage volumes based on the standard curve. The standard curve was generated by adding 0, 0.5, 1, 2, 4, 8 μL autologous blood to 500 μL lysates of same volume and weight of the contralateral brain and the optical density was measured. ICH volumes were extrapolated from the standard curve by linear regression analyses.

Statistical analyses.

All data are presented as mean ± SEM, scatter plots with medians, or box-and-whisker plots. Differences between the means of two groups were assessed by the two-tailed Student's *t* test. For data with Gaussian distributions, differences between means of multiple groups were analyzed by one or two-way ANOVA, followed by the Tukey or Bonferroni *post hoc* test. The Mann-Whitney U test or Kruskal Wallis test was employed when the data distribution was not Gaussian. Two-tailed Pearson correlation analyses were also employed. A *p* value less than or equal to 0.05 was deemed statistically significant. All statistics are summarized in *SI Appendix*, Table S1.

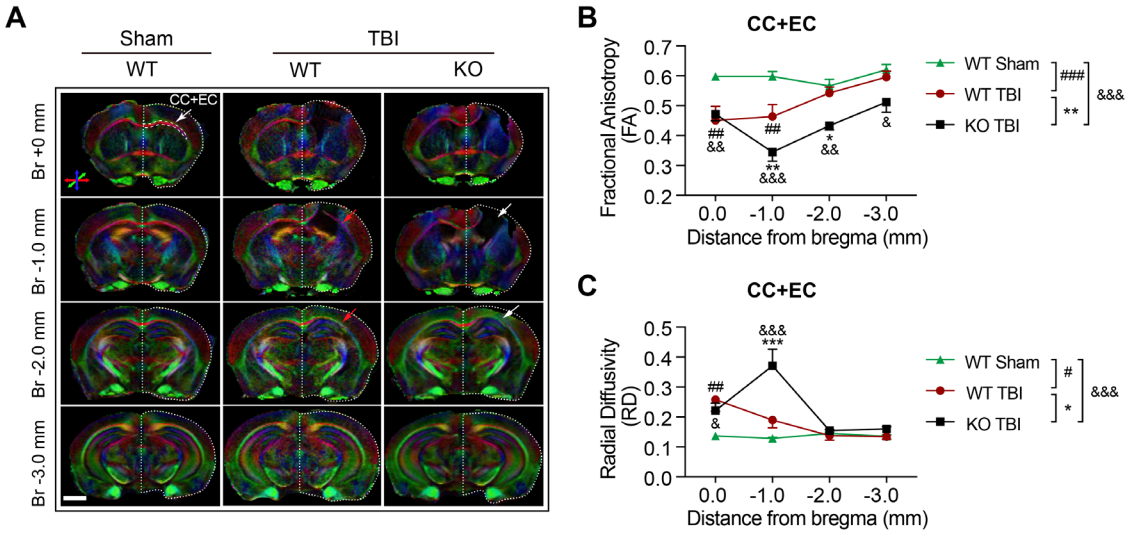

Fig. S1. Diffusion tensor imaging of water diffusion along white matter tracts at 35 days post-TBI. WT and tPA KO mice were subjected to sham injury or unilateral TBI in the right hemisphere. (*A*) Representative directionally-encoded color (DEC) map showing 4 consecutive axial images (interval of 1 mm) from the *ex vivo* brains of WT sham, WT TBI, and KO TBI mice. After TBI, the color intensity is decreased in the corpus callosum and external capsule (arrows: CC+EC). Scale bar, 1.5 mm. (*B* and *C*) Quantification of FA and RD values in four images at indicated distances from Bregma. Data are presented as mean ± SEM, n=4 per group. $^{\#}p\leq0.05$, $^{\#\#}p\leq0.01$, $^{\#\#\#}p\leq0.001$ WT TBI vs. WT Sham, $^{*}p\leq0.05$, $^{**}p\leq0.01$, $^{***}p\leq0.001$ KO TBI vs. WT TBI, $^{\&}p\leq0.05$, $^{\&\&}p\leq0.01$, $^{\&\&\&}p\leq0.001$ KO TBI vs. WT Sham according to a two-way ANOVA followed by the Tukey *post hoc* correction.

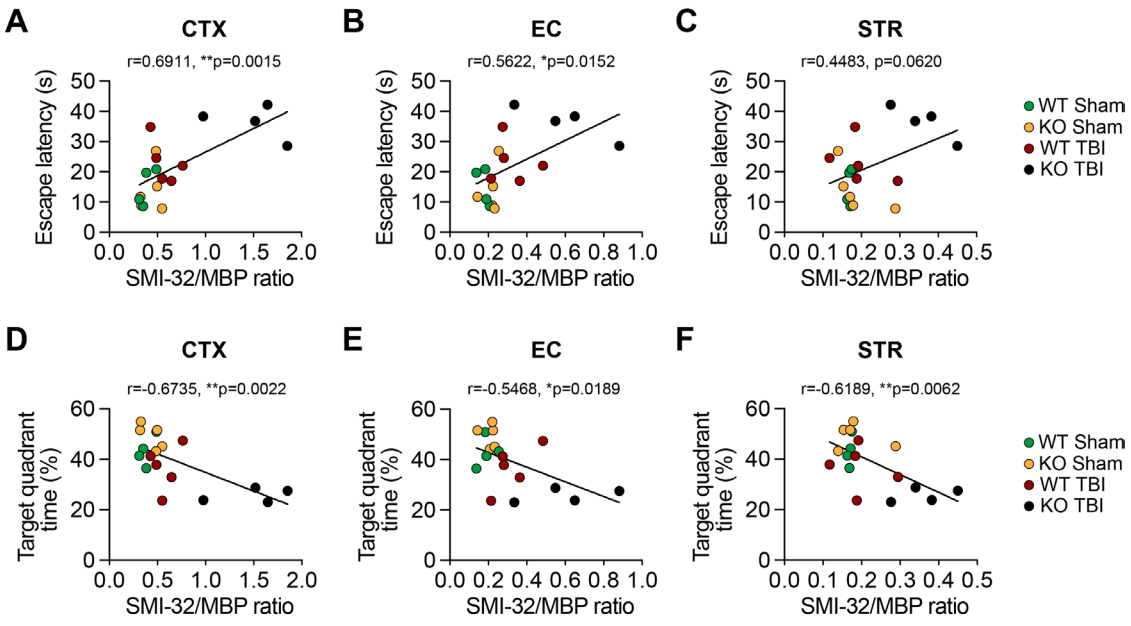

Fig. S2. Correlation between white matter injury markers and long-term cognitive dysfunction after TBI. WT and tPA KO mice were subjected to sham injury or TBI in the right hemisphere. Correlation analyses were conducted to assess the relationship between the ratio of SMI-32 to MBP fluorescent intensity in the cortex (CTX), external capsule (EC), and striatum (STR) and the escape latency in the water maze learning test (*A-C*) on day 33 post-TBI or the time spent in the target quadrant during the water maze memory test (*D-F*) on day 34 post TBI or sham surgery. n=4-5/group. *p≤0.05, **p≤0.01 by two-tailed Pearson product linear correlation analyses.

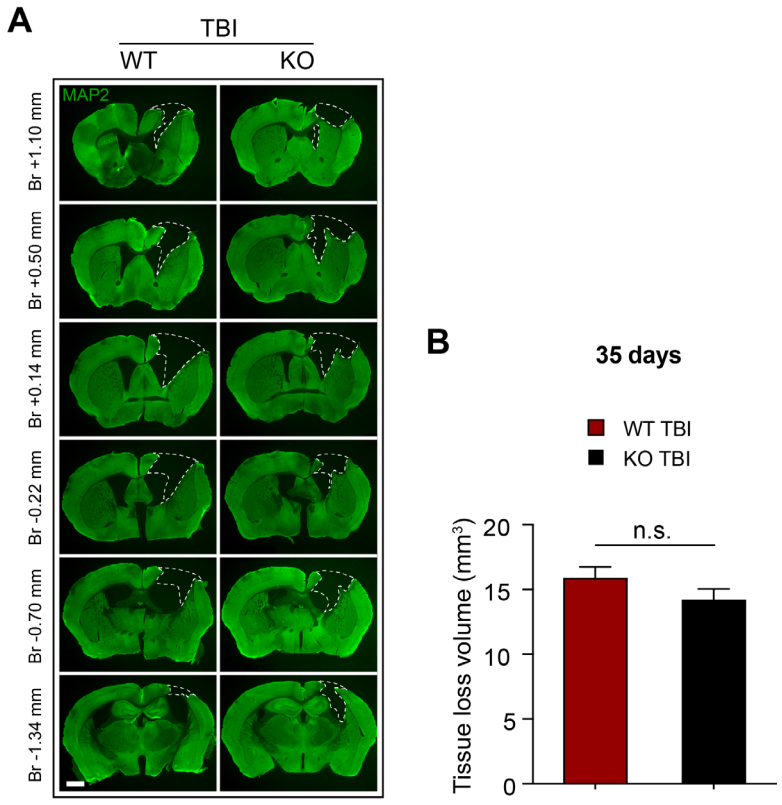

Fig. S3. tPA knockout and wildtype mice exhibit comparable focal tissue loss after TBI. WT and tPA KO mice were subjected to sham injury or unilateral TBI in the right hemisphere. (*A*) Six coronal sections spanning from 1.10 mm anterior to Bregma (Br +1.10 mm) to 1.34 mm posterior to Bregma (Br -1.34 mm) were stained with the neuronal somatodendritic marker MAP2 at 35 days post-TBI. The dashed line defines the border of the zone of tissue loss. Scale bar, 1 mm. (*B*) Quantification of focal tissue loss volume, defined as the viable tissue volume of the ipsilateral hemisphere subtracted from the viable tissue volume of the contralateral hemisphere. Data are presented as mean ± SEM, n=13 per group. n.s. no significant difference by Student's *t*-test.

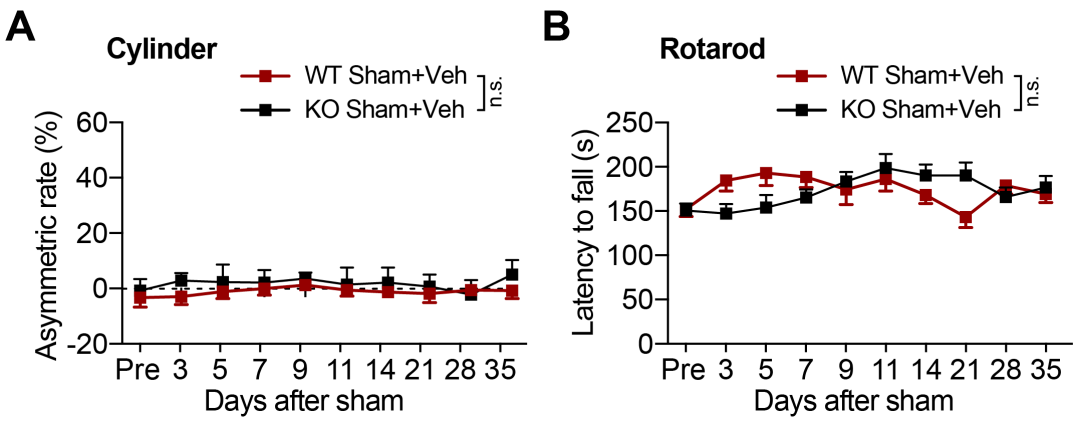

Fig. S4. Wildtype and tPA knockout mice exhibit no changes in sensorimotor function up to 35 days after sham operation. WT and tPA KO mice were subjected to sham operation and subsequently treated with intranasal vehicle infusions with the same regimen as tPA, in parallel with the latter group. The cylinder (*A*) and rotarod (*B*) tests were performed to assess forelimb use asymmetry and sensorimotor coordination up to 35 days after sham operation. Sham operation elicits no effect on asymmetry and rotarod performance. Furthermore, animals experience no significant learning on the rotarod over the entire testing period. Data are presented as mean ± SEM, n=8-9 per group. n.s. no significant difference by two-way repeated ANOVA.

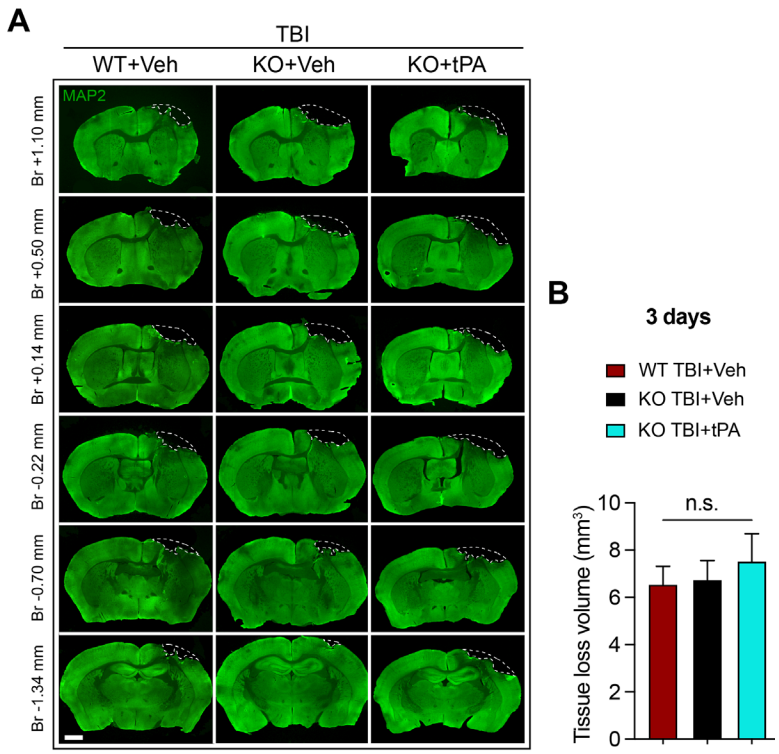

Fig. S5. Neither endogenous nor exogenous tPA *acutely* modifies focal tissue loss at the site of contusion 3 days after TBI. WT and tPA KO mice were subjected to unilateral TBI in the right hemisphere. tPA (0.5 mg/kg) or an equivalent volume of vehicle (PBS) was delivered intranasally 2 h after TBI and on day 2 post injury. (*A*) Representative images of MAP2 staining from WT+Veh, KO+Veh, and KO+tPA groups 3 days after TBI. Scale bar, 1 mm. (*B*) Quantification of tissue loss volume. Sham mice exhibited no tissue loss and are not shown. Data are presented as mean ± SEM, n=5-6 per group. n.s. no significant difference by one-way ANOVA.

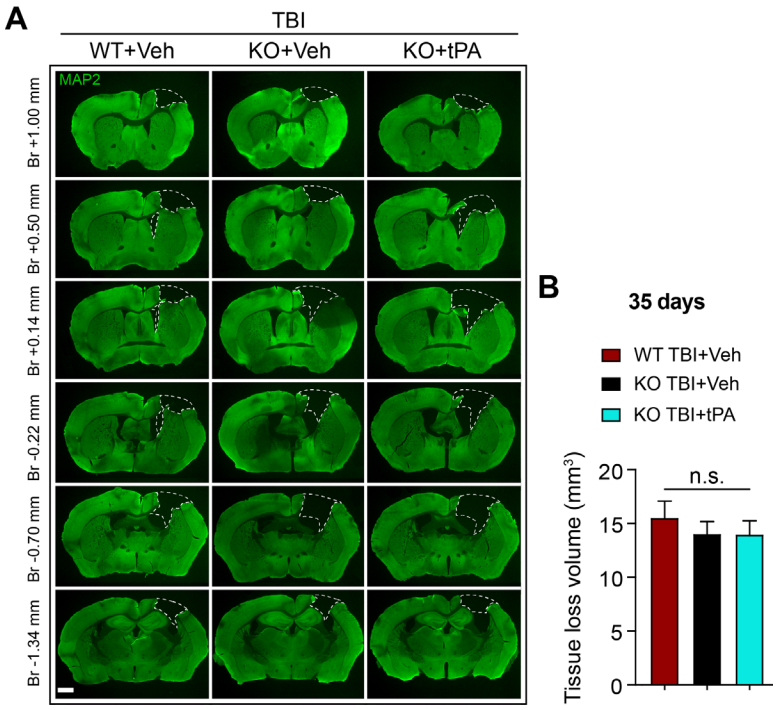

Fig. S6. Neither endogenous nor exogenous tPA modifies focal tissue loss at the site of contusion 35 days after TBI. WT and tPA KO mice were subjected to sham operation or unilateral TBI in the right hemisphere. Sham surgery caused no tissue loss and is not shown here. tPA (0.5 mg/kg) or an equivalent volume of vehicle (PBS) was delivered intranasally 2 h after TBI and every other day up to 14 days post-injury. (*A*) Representative images of MAP2 staining from WT+Veh, KO+Veh, and KO+tPA groups on day 35 after TBI. Scale bar, 1 mm. (*B*) Quantification of tissue loss volume. Data are presented as mean ± SEM, n=7-8 per group. n.s. no significant difference by one-way ANOVA.

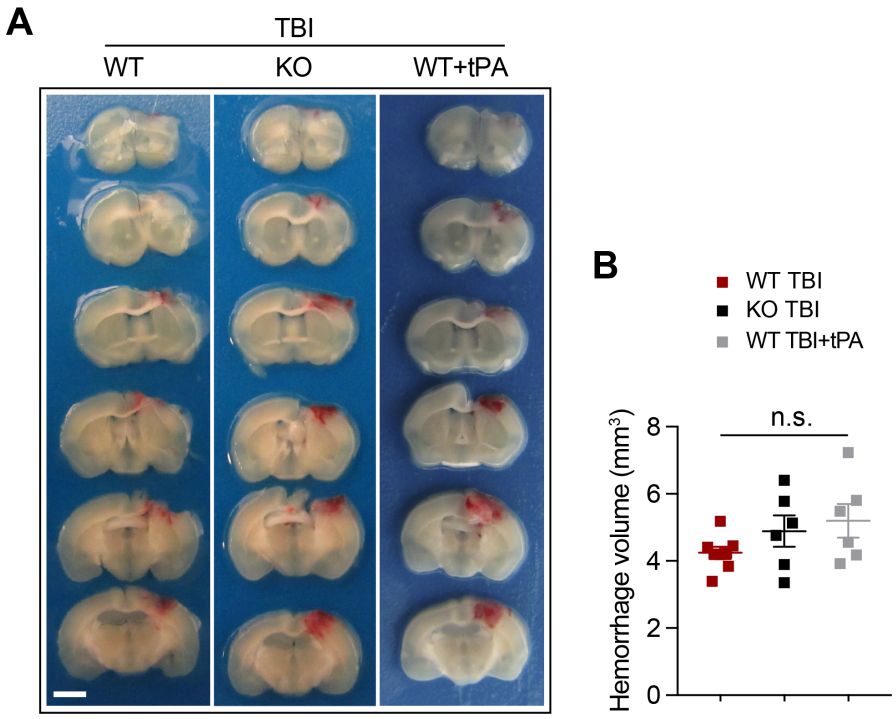

Fig. S7. Comparable intracranial hemorrhage in tPA knockout, wildtype, and recombinant tPA-treated wildtype mice 24 hours after TBI. WT and tPA KO mice were subjected to TBI in the right hemisphere and tPA (0.5 mg/kg) was given intranasally to WT mice 2 h after TBI and 2 h before sacrifice to maximize the chances of observing hemorrhage. (*A*) Representative images of coronal sections displaying intracranial hemorrhage. Scale bar, 2 mm. (*B*) Blinded quantification of total hemorrhage volume based on the photographed brain coronal sections as shown in *A*. Data are presented as mean ± SEM. n=6-8 per group. n.s. no significant difference by one-way ANOVA.

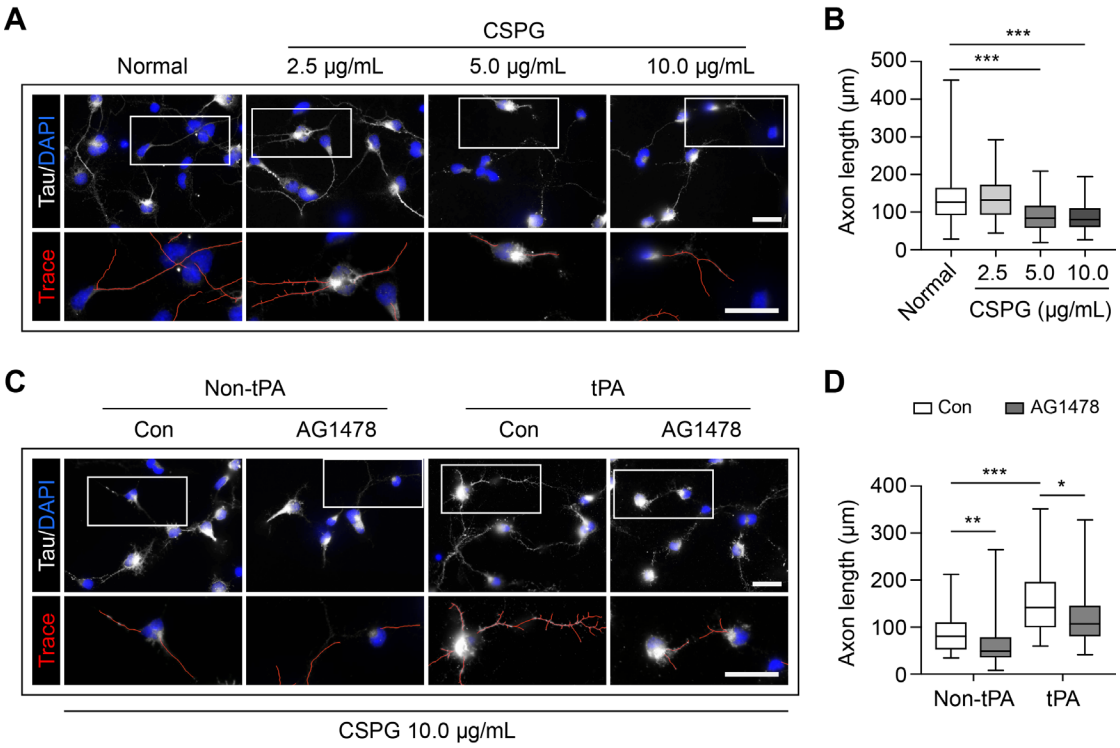

Fig. S8. tPA promotes neurite outgrowth in cortical neuron cultures. (*A* and *B*) Cultured primary neurons were plated on coverslips previously coated with increasing concentrations of chondroitin sulfate proteoglycan (CSPG) and fixed and stained for the axonal marker tau 24 h later. See Supplemental Methods. (*A*) Representative images of tau immunostaining (white) and nuclei (DAPI, blue) staining (upper row); representative images of automated neurite trace from the boxed regions in the upper row (lower row). Scale bar, 150 µm. (*B*) Quantification of axon length by a blinded observer. Rank data represent 100-105 micrographs per group from 3 independent studies. Axon outgrowth was significantly reduced by 5 µg/mL and 10 µg/mL of CSPG. (*C* and *D*) The EGFR blocker AG1478, tPA (10 ng/mL), or their respective vehicles were added to the same culture system as in *A* and *B*. Scale bar, 150 µm. (*D*) Quantification of axon length from 101-110 neurons per group in 3 independent studies. tPA increases axonal outgrowth in the presence of CSPG. The EGFR blocker AG1478 reduces the outgrowth induced by exogenous tPA and may also reduce outgrowth by acting on endogenous tPA. Data are presented as box and whisker plots showing the 25th, 50th, and 75th percentiles and the maximum and minimum values. *p≤0.05, **p≤0.01, ***p≤0.001 by the Kruskal-Wallis test.

Table S1. Statistical table.

	Description	Days after TBI or Sham surgery	in vivo or in vitro	Test used	Stat-value	One- or two-tailed P value?
Fig1. A	Cylinder test	Pre-35d	in vivo	Two-way repeated ANOVA	F (1, 16) = 0.03543, P=0.8531 (bracket, WT Sham vs. KO Sham)	two-tailed
Fig1. A	Cylinder test	Pre-35d	in vivo	Two-way repeated ANOVA	F (1, 20) = 9.941, P=0.0050 (bracket, WT TBI vs. KO TBI); Bonferroni post hoc correction, P=0.0210 (day28, WT TBI vs. KO TBI)	two-tailed
Fig1. B	Rotarod test	Pre-35d	in vivo	Two-way repeated ANOVA	F (1, 16) = 0.1365, P=0.7166 (bracket, WT Sham vs. KO Sham)	two-tailed
Fig1. B	Rotarod test	Pre-35d	in vivo	Two-way repeated ANOVA	F (1, 21) = 7.081, P=0.0146 (bracket, WT TBI vs. KO TBI); Bonferroni post hoc correction, P=0.0029 (day3, WT TBI vs. KO TBI)	two-tailed
Fig1. E	Morris water maze learning test	29d-33d	in vivo	Two-way repeated ANOVA	F (1, 18) = 2.332, P=0.1441 (bracket, WT Sham vs. KO Sham)	two-tailed
Fig1. F	Morris water maze learning test	29d-33d	in vivo	Two-way repeated ANOVA	F (1, 21) = 8.539, P=0.0081 (bracket, WT TBI vs. KO TBI); Bonferroni post hoc correction, P=0.0283 (day30, WT TBI vs. KO TBI)	two-tailed
Fig1. G	Morris water maze memory test	34d	in vivo	Two-way ANOVA	F (1, 39) = 3.982, P=0.0530 (WT vs. KO); Tukey post hoc correction, P=0.0193 (WT Sham vs. WT TBI); P<0.0001 (KO Sham vs. KO TBI); P=0.0211 (WT TBI vs. KO TBI)	two-tailed
Fig1. H	Morris water maze swimming speed	34d	in vivo	Two-way ANOVA	F (1, 39) = 0.5086, P=0.4800 (WT vs. KO); F (1, 39) = 0.01938, P=0.8900 (Sham vs. TBI)	two-tailed
Fig2. B	Averaged FA value	35d	in vivo	Two-way ANOVA	F (1, 12) = 13.58, P=0.0031 (WT vs. KO); Tukey post hoc correction, P=0.0036 (WT TBI CL vs. WT TBI IL); P<0.0001 (KO TBI CL vs. KO TBI IL); P=0.0011 (WT TBI IL vs. KO TBI IL)	two-tailed
Fig2. B	Averaged RD value	35d	in vivo	Two-way ANOVA	F (1, 12) = 10.89, P=0.0063 (WT vs. KO); Tukey post hoc correction, P<0.0001 (KO TBI CL vs. KO TBI IL); P=0.0026 (WT TBI IL vs. KO TBI IL)	two-tailed
Fig2. D	SMI-32/MBP ratio in CTX	35d	in vivo	Two-way ANOVA	F (1, 35) = 43.3, P<0.0001 (WT vs. KO); Tukey post hoc correction, P<0.0001 (WT TBI vs. KO TBI); P<0.0001 (KO Sham vs KO TBI)	two-tailed
Fig2. D	SMI-32/MBP ratio in EC	35d	in vivo	Two-way ANOVA	F (1, 34) = 6.794, P=0.0135 (WT vs. KO); Tukey post hoc correction, P=0.0019 (WT TBI vs. KO TBI); P<0.0001(KO Sham vs KO TBI)	two-tailed
Fig2. D	SMI-32/MBP ratio in STR	35d	in vivo	Two-way ANOVA	F (1, 34) = 4.171, P=0.0489 (WT vs. KO); Tukey post hoc correction, P=0.0102 (WT TBI vs. KO TBI); P=0.0220 (KO Sham vs KO TBI)	two-tailed

Fig2. E	Correlation between SMI-32/MBP ratio in CTX and cylinder test	35d	in vivo	Pearson Product linear regression analyses	r=0.5579, **P=0.0070; Y = 0.1638*X + 0.02257	two-tailed
Fig2. F	Correlation between SMI-32/MBP ratio in EC and cylinder test	35d	in vivo	Pearson Product linear regression analyses	r=0.4272, *P=0.0474; Y = 0.5643*X - 0.01042	two-tailed
Fig2. G	Correlation between SMI-32/MBP ratio in STR and cylinder test	35d	in vivo	Pearson Product linear regression analyses	r=0.1702, P=0.4488; Y = 0.08564*X + 0.1121	two-tailed
Fig2. H	Correlation between SMI-32/MBP ratio in CTX and rotarod test	35d	in vivo	Pearson Product linear regression analyses	r=-0.6849, ***P=0.0004; Y = -60.04*X + 188.9	two-tailed
Fig2. I	Correlation between SMI-32/MBP ratio in EC and rotarod test	35d	in vivo	Pearson Product linear regression analyses	r=-0.5565, **P=0.0072; Y = -219.5*X + 204.2	two-tailed
Fig2. J	Correlation between SMI-32/MBP ratio in STR and rotarod test	35d	in vivo	Pearson Product linear regression analyses	r=-0.2473, P=0.2671; Y = -37.16*X + 157.6	two-tailed
Fig3. B	β-APP density in CC	3d	in vivo	Two-way ANOVA	F (1, 23) = 0.6841, P=0.4167 (WT vs. KO) Tukey post hoc correction, P<0.0001 (WT Sham vs. WT TBI); P<0.0001 (KO Sham vs. KO TBI); P=0.6092 (WT TBI vs. KO TBI)	two-tailed
Fig3. B	β-APP density in EC	3d	in vivo	Two-way ANOVA	F (1, 21) = 13.87, P=0.0013 (WT vs. KO) Tukey post hoc correction, P=0.0010 (WT Sham vs. WT TBI); P<0.0001 (KO Sham vs. KO TBI); P=0.0001 (WT TBI vs. KO TBI)	two-tailed
Fig3. B	β-APP density in STR	3d	in vivo	Two-way ANOVA	F (1, 22) = 10.1, P=0.0044 (WT vs. KO) Tukey post hoc correction, P=0.0060 (WT Sham vs. WT TBI); P<0.0001 (KO Sham vs. KO TBI); P=0.0001 (WT TBI vs. KO TBI)	two-tailed
Fig3. E	SMI-32/MBP ratio in CTX	3d	in vivo	t-test	t (8)=2.492, P=0.0374 (WT TBI vs. KO TBI)	two-tailed
Fig3. E	SMI-32/MBP ratio in EC	3d	in vivo	t-test	t (9)=4.756, P=0.0010 (WT TBI vs. KO TBI)	two-tailed
Fig3. E	SMI-32/MBP ratio in STR	3d	in vivo	t-test	t (9)=3.649, P=0.0053 (WT TBI vs. KO TBI)	two-tailed
Fig3. H	Evoked CAPs	3d	in vivo	Two-way repeated ANOVA	F (1, 11) = 0.1043, P=0.7528 (bracket, WT Sham vs. KO Sham)	two-tailed
Fig3. H	Evoked CAPs	3d	in vivo	Two-way repeated ANOVA	F (1, 15) = 6.89, P=0.0191 (bracket, WT TBI vs. KO TBI); Bonferroni post hoc correction, P=0.0092 (500μA), P=0.0078 (750μA), P=0.0058 (1000μA), P=0.0295 (1250μA)	two-tailed

Fig4. A	Cylinder test	Pre-35d	in vivo	Two-way repeated ANOVA	F (2, 27) = 4.739, P=0.0172 (WT TBI+Veh, KO TBI+Veh, and KO TBI+tPA); Tukey post hoc correction, P=0.0367 (bracket, WT TBI+Veh vs. KO TBI+Veh), P=0.0303 (bracket, KO TBI+Veh vs. KO TBI+tPA); P=0.0167 (day9, KO TBI+Veh vs. KO TBI+tPA), P=0.0250 (day14, WT TBI+Veh vs. KO TBI+Veh), P=0.0439 (day21, WT TBI+Veh vs. KO TBI+Veh)	two-tailed
Fig4. B	Rotarod test	Pre-35d	in vivo	Two-way repeated ANOVA	F (2, 28) = 6.331, P=0.0054 (WT TBI+Veh, KO TBI+Veh, and KO TBI+tPA); Tukey post hoc correction, P=0.0076 (bracket, WT TBI+Veh vs. KO TBI+Veh), P=0.0257 (bracket, KO TBI+Veh vs. KO TBI+tPA); P=0.0260 (day5, WT TBI+Veh vs. KO TBI+Veh), P=0.0006 (day7, WT TBI+Veh vs. KO TBI+Veh), P=0.0004 (day9, WT TBI+Veh vs. KO TBI+Veh), P=0.0053 (day9, KO TBI+Veh vs. KO TBI+tPA), P=0.0010 (day11, WT TBI+Veh vs. KO TBI+Veh), P=0.0268 (day11, KO TBI+Veh vs. KO TBI+tPA), P=0.0029 (day14, WT TBI+Veh vs. KO TBI+Veh), P=0.0025, (day14, KO TBI+Veh vs. KO TBI+tPA)	two-tailed
Fig4. C	Morris water maze learning test	29d-33d	in vivo	Two-way repeated ANOVA	F (2, 30) = 8.175, P=0.0015 (WT TBI+Veh, KO TBI+Veh, and KO TBI+tPA); Tukey post hoc correction, P=0.0041 (bracket, WT TBI+Veh vs. KO TBI+Veh), P=0.0072 (day31, WT TBI+Veh vs. KO TBI+Veh), P=0.0045 (day33, WT TBI+Veh vs. KO TBI+Veh)	two-tailed
Fig4. D	Morris water maze memory test	34d	in vivo	One-way ANOVA	F (2, 30)=7.207, P=0.0028 (WT TBI+Veh, KO TBI+Veh, and KO TBI+tPA); Tukey post hoc correction, P=0.0058 (WT TBI+Veh vs. KO TBI+Veh); P=0.0110 (KO TBI+Veh vs. KO TBI+tPA)	two-tailed
Fig4. E	Morris water maze swimming speed	34d	in vivo	Kruskal-Wallis test	P=0.8096	two-tailed
Fig5. B	SMI-32/MBP ratio in CTX	35d	in vivo	One-way ANOVA	F (2, 25) = 7.125, P=0.0036 (WT TBI+Veh, KO TBI+Veh, and KO TBI+tPA); Tukey post hoc correction, P=0.0488 (WT TBI+Veh vs. KO TBI+Veh); P=0.0032 (KO TBI+Veh vs. KO TBI+tPA)	two-tailed
Fig5. C	SMI-32/MBP ratio in EC	35d	in vivo	One-way ANOVA	F (2, 25) = 6.303, P=0.0061 (WT TBI+Veh, KO TBI+Veh, and KO TBI+tPA); Tukey post hoc correction, P=0.0130 (WT TBI+Veh vs. KO TBI+Veh); P=0.0168 (KO TBI+Veh vs. KO TBI+tPA)	two-tailed

Fig5. D	SMI-32/MBP ratio in STR	35d	in vivo	One-way ANOVA	F (2, 26) = 1.225, P=0.3101 (WT TBI+Veh, KO TBI+Veh, and KO TBI+tPA); Tukey post hoc correction, P=0.3293 (WT TBI+Veh vs. KO TBI+Veh); P=0.9364 (KO TBI+Veh vs. KO TBI+tPA)	two-tailed
Fig5. F	Evoked CAPs	35d	in vivo	Two-way repeated ANOVA	F (2, 28) = 2.815, P=0.0769 (WT TBI+Veh, KO TBI+Veh, and KO TBI+tPA); Tukey post hoc correction, P=0.0468 (500μA), P=0.0247 (750μA), P=0.0094 (1000μA), P=0.0042 (1250μA), P=0.0061 (1500μA), P=0.0059 (1750μA), P=0.0028 (2000μA) (KO TBI+Veh vs KO TBI+tPA); P=0.0474 (1250μA), P=0.0475 (1750μA), P=0.0349 (2000μA) (WT TBI+Veh vs. KO TBI+Veh).	two-tailed
Fig5. G	Correlation between SMI-32/MBP ratio in CTX and evoked CAPs	35d	in vivo	Pearson Product linear regression analyses	r=-0.557, **P=0.0058; Y = -0.4027*X + 0.8795	two-tailed
Fig5. H	Correlation between SMI-32/MBP ratio in EC and evoked CAPs	35d	in vivo	Pearson Product linear regression analyses	r=-0.4948, *P=0.0164; Y = -1.526*X + 0.9877	two-tailed
Fig5. I	Correlation between SMI-32/MBP ratio in STR and evoked CAPs	35d	in vivo	Pearson Product linear regression analyses	r=-0.2912, P=0.1777; Y = -0.3486*X + 0.6929	two-tailed
Fig5. J	Correlation between evoked CAPs and cylinder test	35d	in vivo	Pearson Product linear regression analyses	r=-0.6254, ***P=0.0004; Y = -0.26*X + 0.3252	two-tailed
Fig5. K	Correlation between evoked CAPs and rotarod test	35d	in vivo	Pearson Product linear regression analyses	r=0.7102, ***P<0.0001; Y = 82.9*X + 89.41	two-tailed
Fig6. B	β-APP density in EC	35d	in vivo	One-way ANOVA	F (2, 14) = 4.736, P=0.0268 (WT TBI+Veh, KO TBI+Veh, and KO TBI+tPA); Tukey post hoc correction, P=0.0488 (WT TBI+Veh vs. KO TBI+Veh), P=0.0463 (KO TBI+Veh vs. KO TBI+tPA)	two-tailed
Fig6. B	β-APP density in STR	35d	in vivo	One-way ANOVA	F (2, 13) = 6.672, P=0.0101 (WT TBI+Veh, KO TBI+Veh, and KO TBI+tPA); Tukey post hoc correction, P=0.0242 (WT TBI+Veh vs. KO TBI+Veh), P=0.0182 (KO TBI+Veh vs. KO TBI+tPA)	two-tailed

Fig6. D	Intracranial hemorrhage	24h	in vivo	One-way ANOVA	F (2, 17) = 0.5982, P=0.5609 (WT TBI, KO TBI, and WT TBI+tPA); Tukey post hoc correction, P=0.9792 (WT vs. KO), P=0.5530 (WT vs. WT+tPA), P=0.7050 (KO vs. WT+tPA)	two-tailed
Fig7. C	Sprouting axons at C7 level	35d	in vivo	One-way ANOVA	F (4, 23) = 4.429, P=0.0084 (WT Sham+Veh, KO Sham+Veh, WT TBI+Veh, KO TBI+Veh, and KO TBI+tPA); Tukey post hoc correction, P=0.0225 (WT TBI+Veh vs. KO TBI+Veh); P=0.0087 (KO TBI+Veh vs. KO TBI+tPA)	two-tailed
Fig7. C	Sprouting axons at FN level	35d	in vivo	One-way ANOVA	F (4, 24) = 19.43, P<0.0001 (WT Sham+Veh, KO Sham+Veh, WT TBI+Veh, KO TBI+Veh, and KO TBI+tPA); Tukey post hoc correction, P=0.2875 (WT TBI+Veh vs. KO TBI+Veh); P=0.0328 (KO TBI+Veh vs. KO TBI+tPA); P=0.0086 (WT Sham+Veh vs. WT TBI+Veh); P<0.0001 (KO Sham+Veh vs. KO TBI+Veh)	two-tailed
Fig7. D	Correlation between sprouting axons in C7 and cylinder test	35d	in vivo	Pearson Product linear regression analyses	r=-0.54, **P=0.0095; Y = -0.03941*X + 2.559	two-tailed
Fig7. E	Correlation between sprouting axons in C7 and rotarod test	35d	in vivo	Pearson Product linear regression analyses	r=0.5186, *P=0.0134; Y = 0.02673*X - 1.839	two-tailed
FigS1. B	FA value	35d	in vivo	Two-way ANOVA	F (2, 36) = 33.74, P<0.0001 (WT Sham, WT TBI, and KO TBI); Tukey post hoc correction, P=0.0003 (bracket, WT Sham vs. WT TBI); P<0.0001 (bracket, WT Sham vs. KO TBI); P=0.0013 (bracket, WT TBI vs. KO TBI); P=0.0012 (0.0 mm, WT Sham vs. WT TBI); P=0.0054, (0.0 mm, WT Sham vs. KO TBI); P=0.0030 (-1.0 mm, WT Sham vs. WT TBI); P<0.0001 (-1.0 mm, WT Sham vs. KO TBI); P=0.0095 (-1.0 mm, WT TBI vs. KO TBI); P=0.0033 (-2.0 mm, WT Sham vs. KO TBI); P=0.0170 (-2.0 mm, WT TBI vs. KO TBI); P=0.0187 (-3.0 mm, WT Sham vs. KO TBI)	two-tailed

FigS1. C	RD value	35d	in vivo	Two-way ANOVA	F (2, 36) = 15.73, P<0.0001 (WT Sham, WT TBI, and KO TBI); Tukey post hoc correction, P=0.0279 (bracket, WT Sham vs. WT TBI), P<0.0001 (bracket, WT Sham vs. KO TBI), P=0.0165 (bracket, WT TBI vs. KO TBI); P=0.0016 (0.0 mm, WT Sham vs. WT TBI); P=0.0320, (0.0 mm, WT Sham vs. KO TBI); P<0.0001 (-1.0 mm, WT Sham vs. KO TBI); P<0.0001 (-1.0 mm, WT TBI vs. KO TBI)	two-tailed
FigS2. A	Correlation between SMI-32/MBP ratio in CTX and water maze learning test	33d	in vivo	Pearson Product linear regression analyses	r=0.6911, P=0.0015, Y = 15.61*X + 10.92	two-tailed
FigS2. B	Correlation between SMI-32/MBP ratio in EC and water maze learning test	33d	in vivo	Pearson Product linear regression analyses	r=0.5622, P=0.0152, Y = 30.9*X + 11.83	two-tailed
FigS2. C	Correlation between SMI-32/MBP ratio in STR and water maze learning test	33d	in vivo	Pearson Product linear regression analyses	r=0.4483, P=0.0620, Y = 52.65*X + 10.04	two-tailed
FigS2. D	Correlation between SMI-32/MBP ratio in CTX and water maze memory test	34d	in vivo	Pearson Product linear regression analyses	r=-0.6735, P=0.0022, Y = -14.74*X + 49.56	two-tailed
FigS2. E	Correlation between SMI-32/MBP ratio in EC and water maze memory test	34d	in vivo	Pearson Product linear regression analyses	r=-0.5468, P=0.0189, Y = -29.13*X + 48.68	two-tailed
FigS2. F	Correlation between SMI-32/MBP ratio in STR and water maze memory test	34d	in vivo	Pearson Product linear regression analyses	r=-0.6189, P=0.0062, Y = -70.45*X + 55.04	two-tailed
FigS3. B	Tissue loss	35d	in vivo	t-test	t (24)=1.543, P=0.1358	two-tailed
FigS4. A	Cylinder test	35d	in vivo	Two-way repeated ANOVA	F (1, 14) = 0.7374, P=0.4050 (WT Sham+Veh vs KO Sham+Veh)	two-tailed
FigS4. B	Rotarod test	35d	in vivo	Two-way repeated ANOVA	F (1, 15) = 0.01589, P=0.9014 (WT Sham+Veh vs KO Sham+Veh)	two-tailed
FigS5. B	Tissue loss	3d	in vivo	One-way ANOVA	F (2, 14) = 0.3127, P=0.7364 (WT TBI+Veh, KO TBI+Veh, and KO TBI+tPA)	two-tailed
FigS6. B	Tissue loss	35d	in vivo	One-way ANOVA	F (2, 20) = 0.3133, P=0.7346 (WT TBI+Veh, KO TBI+Veh, and KO TBI+tPA)	two-tailed

FigS7. B	Hemorrhage volume	24h	in vivo	One-way ANOVA	F (2, 17) = 1.773, P=0.1998 (WT TBI, KO TBI, and WT TBI+tPA)	two-tailed
FigS8. B	Axon length	/	in vitro	Kruskal-Wallis test	P<0.0001 (Normal, 2.5, 5.0, and 10.0); P<0.0001 (Normal vs. 5.0); P<0.0001 (Normal vs. 10.0)	two-tailed
FigS8. D	Axon length	/	in vitro	Kruskal-Wallis test	P<0.0001 (Normal, 2.5, 5.0, and 10.0); P=0.0014 (Non-tPA Con vs. Non-tPA AG); P<0.0001 (Non-tPA Con vs. tPA Con); P=0.0471 (tPA Con vs. tPA AG)	two-tailed

References

1. National Research Council (2011) *Guide for the Care and Use of Laboratory Animals* (National Academies Press, Washington, DC), 8th Ed.

2. Wang G, et al. (2015) HDAC inhibition prevents white matter injury by modulating microglia/macrophage polarization through the GSK3beta/PTEN/Akt axis. *Proc Natl Acad Sci U S A* 112(9):2853-2858.

3. Shi Y, et al. (2017) Endothelium-targeted overexpression of heat shock protein 27 ameliorates blood-brain barrier disruption after ischemic brain injury. *Proc Natl Acad Sci U S A* 114(7):E1243-E1252.

4. Shi Y, et al. (2016) Rapid endothelial cytoskeletal reorganization enables early blood-brain barrier disruption and long-term ischaemic reperfusion brain injury. *Nat Commun* 7:10523.

5. Jiang X, et al. (2016) A Post-stroke Therapeutic Regimen with Omega-3 Polyunsaturated Fatty Acids that Promotes White Matter Integrity and Beneficial Microglial Responses after Cerebral Ischemia. *Transl Stroke Res* 7(6):548-561.

6. Yeh FC, et al. (2014) Mapping stain distribution in pathology slides using whole slide imaging. *J Pathol Inform* 5(1):1.

7. Chan KC, et al. (2009) MRI of late microstructural and metabolic alterations in radiation-induced brain injuries. *J Magn Reson Imaging* 29(5):1013-1020.

8. Chan KC, Khong PL, Lau HF, Cheung PT, Wu EX (2009) Late measures of microstructural alterations in severe neonatal hypoxic-ischemic encephalopathy by MR diffusion tensor imaging. *Int J Dev Neurosci* 27(6):607-615.

9. Alexander AL, Lee JE, Lazar M, Field AS (2007) Diffusion tensor imaging of the brain. *Neurotherapeutics* 4(3):316-329.

10. Meijering E, et al. (2004) Design and validation of a tool for neurite tracing and analysis in fluorescence microscopy images. *Cytometry A* 58(2):167-176.

11. Pu H, et al. (2013) Omega-3 polyunsaturated fatty acid supplementation improves neurologic recovery and attenuates white matter injury after experimental traumatic brain injury. *J Cereb Blood Flow Metab* 33(9):1474-1484.

12. Hijazi N, et al. (2015) Endogenous plasminogen activators mediate progressive intracerebral hemorrhage after traumatic brain injury in mice. *Blood* 125(16):2558-2567.